Automated Detection and Segmentation of Mitochondrial Images based on Gradient Enhancement and Adaptive Gabor Filter

Nhan Nguyen-Thanh, Tuan Pham, Kazuhisa Ichikawa

Automated Detection and Segmentation of Mitochondrial Images based on Gradient Enhancement and Adaptive Gabor Filter

Nhan Nguyen-Thanh, Tuan D. Pham and Kazuhisa Ichikawa

***Abstract*—Information of cellular organelles location and morphology is essential for cancer simulation. In order to obtain such information, the segmentation of the organelles from electronic microscopy intracellular image is crucial. In this paper, we focus on the automatic segmentation of mitochondria organelle which is one of the most important organelles tightly related to the form of cancer. A simple three-stage strategy which includes coarse segmentation, detection and fine segmentation is proposed for fully automatic mitochondria segmentation. The local gradient calculation provides a weight factor matrix and a orientation matrix. The weight factor matrix will improve the contrast of organelle boundary of intracellular images and hence facilitate both coarse and fine mitochondria segmentation. The orientation matrix will be used for enhancing the Gabor feature extraction which make the mitochodrial detection process more accurate. Machine learning-based classifiers including *k*-nearest neighbor (*k*-NN), support vector machine (SVM)-based and neural network (NN)-based classifiers, are considered to learn with eight extracted features for mitochondrial detection. Experimental results on focused ion beam (FIB) and scanning electron microscope (SEM) images of cancer cellular of human head and neck squamous cell carcinoma (SCC-61) have shown the effectiveness of proposed method.**

***Index Terms*—cell organelles, image segmentation, image processing, mitochondria, gradient boundary enhancement, orientation adaptive, Gabor filter, SCC-61, cancer cell.**

I. Introduction

In cell biology, mitochondrion is one of the main organelles that can be found in most eukaryotic cells. This type of organelle concerns with the roles of energy supply, signaling and control of cellular differentiation, growth and death. It is reported that there is a strong link between the function of mitochondria and cancer. [1]. For example, the function of mitochondria of cancer cell is believed to be altered for resistance apoptosis [2], [3]. This leads the research to target on mitochondria for cancer therapy by changing mitochondrial metabolism or stimulating mitochondrial membrane permeabilization [4]. In addition, it is convinced that there are a relation of mitochondrial morphology and molecular controlling mechanisms during cell death [5], [6] and a connection of mitochondrial dynamics to key signaling cascades [7]. Therefore, obtaining information of location and morphology of mitochondria in intracellular space is very useful for cancer simulation.

Recent progresses on super-resolution electronic microscopy enable us to obtain this information through intracellular image. Some earlier methods such as ion-abrasion (IA) or serial block-face (SFB) can be combined with scanning electron microscopy (SEM), which is well-known for capturing surface characteristics and morphology, to obtain a lower resolution of both intercellular and intracellular space. Lately, the detail complex structure of the cell can be acquired with the combination of SEM and focused ion beam (FIB) technique, which increase the resolution of the scan. As a result, the integrated imaging system FIB-SEM has now been a powerful scientific instrument for the study of biological specimens and soft materials [14].

Automatically analyzing and understanding such kind of intracellular electron microscopy images are not a trivial task since the space of cellular contains a complicated system with variety of organelles possessing various shapes and sizes. There are some recent works that succeeds in segmentation of mitochondria [11]–[13] as well as some other cell organelles [8]–[10]. In detail, in [13], a textural-based Gentle-Boot classifier is trained for detecting mitochondria in electron microscopy images of brain tissue. Similarly, in [12], multiple classifiers including *k*-nearest neighbor algorithm (*k*-NN), support vector machine (SVM) and adaptive boosting algorithm (Adaboost) are used for detecting mitochondria and other organelles of highly pigmented human melanoma (MNT-1) cell based on textural feature. These works were said to be under-utilization of image information, i.e., shape information, and were improved in [11] by considering a graph partitioning scheme incorporated with a learn shape feature method. Though the results of these research are reasonable, the huge load works for training the system could be the most difficulty for implementation.

FIB-SEM intracellular images reveal a great detail structure of the cellular space which includes variety types of organelles such as nucleus, mitochondria, golgi apparatus, endoplasmic recticulum, cytoskeleton, vesicle, etc., with difference sizes, shapes, texture and brightness. The solid distribution of these organelles leads the segmentation task for intracellular images to be very complicated. Furthermore, in cases of images of abnormal cellulars such as cancer cells derived from malignant tumor, the structure and other characteristics of organelles tend to be more sophisticated which can cause the hard segmentation task to be harder. In this paper, images of a cancer cellular of human head and neck squamous cell carcinoma (SCC-61) [15], [16] captured by FIB-SEM system are investigated for segmentation mitochondria for a further cancer simulation. In order to perform this purpose, we consider a simple three-stage strategy, as shown in Fig. 1, for automatically identifying and segmenting mitochondria in intracellular images.

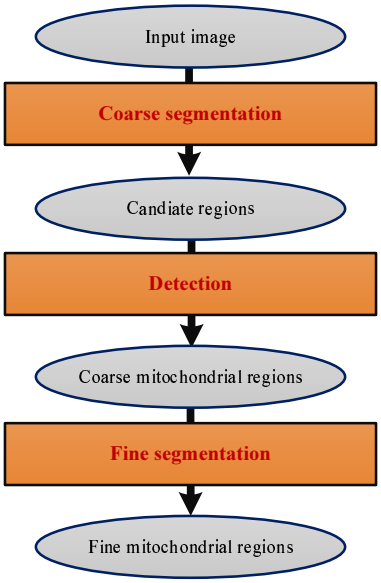

Fig. 1. Mitochondrial segmentation strategy

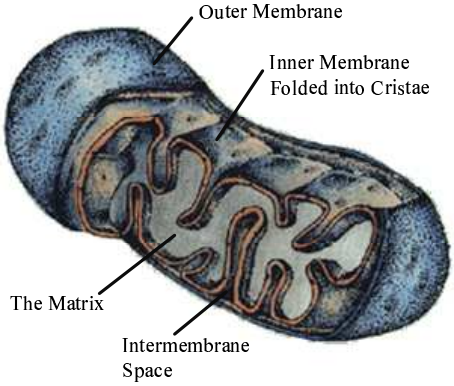

Fig. 2. Mitochondrion picture [38]

First, an initial identification for mitochondria is implemented by coarse segmentation stage. The purpose of this coarse segmentation stage is to identify potential regions which mostly contain mitochondria. This initial identification is mainly based on the characteristic of mitochondrial shape. In other words, the output of this coarse segmentation stage are isolated areas of which the shapes are similar to the shapes of mitochondria,i.e., circular and elliptical forms derived from the cross sections of tubular mitochrodrial structures. As a result, the regions of very small and isolated organelles, which could belong to cytoplasm, free protein or small vesicle, and the regions of complex and sticky filament structures, which can originate from endoplasmic reticulum, golgi apparatus or cytoskeleton organelles, should be excluded principally. Since it is just a coarsely initial segmentation, the requirement of accuracy is not too strict. A simple combination of morphological operators are adopted to perform this task. For facilitating this coarse mitochondrial segmentation stage, a gradient boundary enhancement process, which is implemented based on a weight factor matrix formulated by the gradient magnitude of the mean transformed intracellular image, is additionally considered.

Second, the coarse segmented or candidate regions are further identified to mitochondrial and non-mitochondrial regions based on detection stage. The Gabor features and some basis features such as intensity, perimeter, and areas are extracted for mitochondrial detection stage. The gradient orientation of the mean transformed intracellular image is utilized for extracting orientation adaptive Gabor features which makes the mitochodrial detection process more accurate. In order to combine the eight proposed features for mitochondrial detection, we consider multiple types of machine learning-based classifiers including *k*-nearest neighbor (*k*-NN), support vector machine (SVM)-based and neural network (NN)-based classifiers. Since the accuracy of the three-stage segmentation method is decided in this stage, the main contribution of this paper is concentrated on this part.

Third, the detected coarse mitochondrial regions are finely segmented by fine segmentation stage. The task of this fine segmentation stage is to improve the mitochondrial segmentation by removing non-mitochondrial pixels which touch in coarse mitochondrial regions. Since the input coarse segmented regions of this stage are quite isolated and small, various kind of segmentation methods can be adopted for this stage. Herein, we adopt similar gradient boundary enhancement and combination of morphological operators, used in previous coarse segmentation stage, for performing this improving segmentation task.

The remainder of this paper is organized as follows. In section II, the coarse segmentation stage is described. In section III, the mitochondrial detection strategy is presented in detail. In section IV, the fine segmentation stage is explained. In section V, experiment results are discussed. Finally, in section VI, conclusions are drawn.

II. Coarse and fine segmentation

Fig. 2 illustrates structure of a mitochondrion. It can be seen that the thin outer membrane and cristae, formed by inner membranes will create thin boundaries and ridge structures in mitochondrial scans. An example of cropped FIB-SEM image of intracellular space, as shown in Fig. 4a, reveals that the space is filled by various types organelles with different sizes, shapes and brightness. These organelles are mixed together and their boundaries may not be clear. As a result, the boundary separation or boundary enhancement should be considered as a pre-processing step to facilitate the segmentation task for these organelles. Herein, we focus on thin mitochondrial boundary enhancement by adopting gradient transform.

A. Gradient transform and gradient boundary enhancement

An image I is firstly transformed such that the boundary of interested region is still preserved while the texture inside that region is suppressed. The mean filter, which is computed by

$$\mu_w\left(I_{xy}\right) = \frac{1}{w^2}\sum_w\sum_w I_{xy}, \tag{1}$$

where w is the window size, satisfies this requirement since it smooths texture regions while provides an average intensity

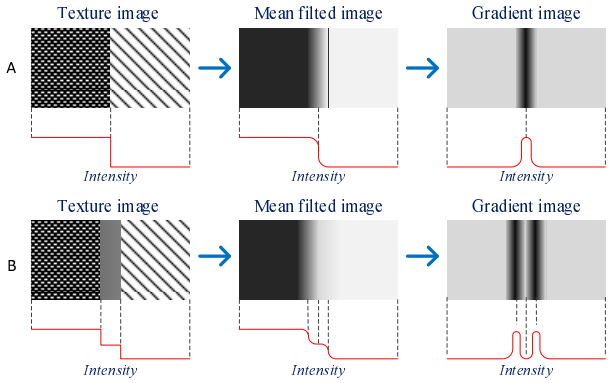

Fig. 3. Gradient boundary *(A)* and ridge *(B)* detection examples

level at the intersection boundary between two difference neighbor textural regions.

Next, the gradient transform vector of the mean transformed image is calculated by

$$\nabla I_{xy} = \left[\frac{\partial I_{xy}}{\partial x}, \frac{\partial I_{xy}}{\partial y}\right] \tag{2}$$

Consequently, the gradient orientation and magnitude at each pixel are computed by

$$\varphi_{xy} = \tan^{-1}\left(\frac{\partial I_{xy}}{\partial y} \Big/ \frac{\partial I_{xy}}{\partial x}\right) \tag{3}$$

and

$$|\nabla I_{xy}| = \sqrt{\left(\frac{\partial I_{xy}}{\partial x}\right)^2 + \left(\frac{\partial I_{xy}}{\partial y}\right)^2}, \tag{4}$$

respectively. The low intensity variation of the smoothed region causes a low gradient value while strong variation between intersection boundary and both neighbor textural region provides two new high gradient value boundaries which limit the original intersection boundary. Therefore, the value of w will determine the thickness of detected boundary. Fig. 3 illustrated the examples of gradient boundary and ridge detection. It can be seen that the gradient transform magnitude provides a good localization for boundaries between textural regions.

In order to perform boundary enhancement, gradient magnitude vector is adopted for formulating a weight factor matrix as follows:

$$W_{xy} = \left(1 - \frac{|\nabla I_{xy}|}{\max\limits_{xy}(|\nabla I_{xy}|)}\right)^n \tag{5}$$

where n is the power transform order, which amplifies the contrast of gradient image. A larger value of n provide a higher contrast of weight factor matrix. The intensity of the original image is directly adjusted by multiplying with the weight factor matrix. In general, the value of n determine the separation level of boundary. A higher value of n can lead to more broken boundary. Therefore, the selection of n is a trade off between the separation of inter-organelle touched objects and the integrity of intra-organelle parts.

B. Mitochondrial coarse segmentation

After adopting enhancement, intracellular images is processed to obtain coarse segmented images by the following steps:

- *Convert to binary images.* A threshold based on Otsu method [18] is used for getting binary version of each enhanced intracellular image.
- *Remove small regions.* Isolated small regions in binary images which could belong to cytoplasm, free protein or small vesicle are removed.
- *Remove nucleus and cell membrane region.*
- *Apply combination of morphological operators.* The combination of morphology operators aiming to keep circular and elliptical shape is described as follows:
  - Fill holes,
  - Apply opening operator with disk structuring element,
  - Remove small regions,
  - Compute erosion by disk structuring element,
  - Remove small regions,
  - And compute dilation by disk structuring element.

Since the morphological operators are adopted to a large area with various condition, the morphological operators is principally selected such that the integrity of mitochondrial organelles is warranty. This selection means that a level of merged objects is acceptable.

Fig. 4 shows a comparison example of coarse mitochondrial segmentation outputs for different enhancement types. Fig 4b is the coarse segmentation output of the original intracellular image in Fig 4a. Fig 4c exhibits the enhanced version based on contrast limited adaptive histograph equalization (CLAHE) [37] of the original intracellular image. Fig 4d gives the coarse segmentation regions obtaining by adopting the proposed algorithm to Fig 4c. Similarly, Fig 4f displays the coarse segmentation regions of the gradient boundary enhanced intracellular image shown in Fig 4e. It can be seen that for the same coarse segmentation algorithm, the gradient boundary enhanced image provide a better coarse segmentation result compared to original non-enhanced image and CLAHE-based enhanced image. Furthermore, since mitochondria are contained in most of coarse segmented regions, a further identification for mitochondrial regions will be implemented in the next detection stage.

C. Mitochondrial fine segmentation

The fine segmentation stage is executed for finely segmenting detected coarse segmented mitochondrial regions. Due to the separation of detected coarse mitochondrial regions, various segmentation method can be applied to provide a fine segmented output without affecting other areas. Therefore, the fine segmentation stage is totally opened for multiple segmentation methods.

Herein, a similar gradient boundary enhancement and morphological operator combination, used in previous coarse segmentation stage, are performed for finely segmenting mitochondria. However, unlike coarse segmentation stage, of gradient boundary enhancement and morphological operators are

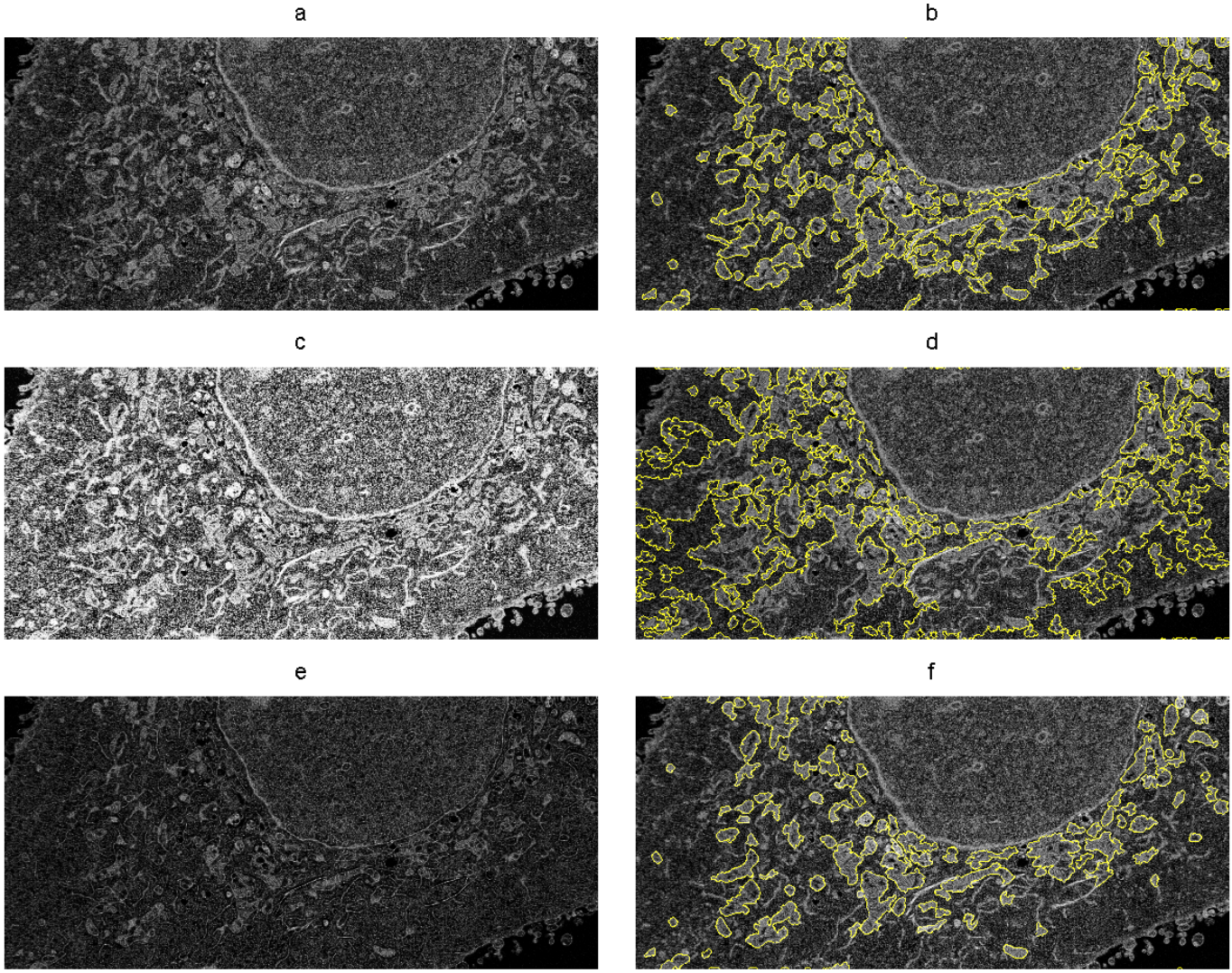

Fig. 4. Coarse segmentation comparison examples. *(a)* An original intracellular image. *(b)* Coarse segmentation of (a). *(c)* Enhanced image of (a) based on CLAHE [37]. *(d)* Coarse segmentation of (c). *(e)* Enhanced image of (a) based on gradient boundary enhancement. *(f)* Coarse segmented image of (e).

only affect in small detected mitochondrial regions. Therefore, the parameters are selected such that a good fine segmentation result can be obtained.

Two examples of fine segmentation results are illustrated in Fig. 5c and 5f. It can be seen that the fine segmentation results are largely improved compared to coarse segmented versions of these objects which are shown in Fig. 5a and 5b.

III. Detection

A. Feature extraction

Extracting an efficient feature set is a crucial for any detection algorithm. A good feature set will provide a good classification result. In this work, the feature set is utilized for determining whether a coarse segmented region contains mitochondria. The best feature for discriminating a mitochrondion from other types of organelles is the ridge texture feature formed by the cross section of cristae. In addition, since the coarse segmented regions can be any types of organelles, some basic features such as intensities, perimeter, area, etc, can provide a certain accuracy level for detecting mitochondria. As a result, we select the feature set that specifies a mitochondrial region mainly based on texture features and some basic regional properties as shown in Fig. 6.

1) Orientation adaptive Gabor filter and Gabor features: Gabor filter is selected for extracting textural feature which objects to ridge structure of mitochondria. The reason for choosing Gabor filter is due to the fact that Gabor filtering is well-known as an invariant and effective method for extracting textural features [19]–[22]. Furthermore, Gabor filter is convinced to be well-adapted to fiber or ridge textural extraction which was contained in variety applications such as fingerprint classification [26], [27], Iris recognition [28]–[30], prostate cancer image segmentation and recognition [31], [32], blood vessel detection [25], character recognition [23], [24]. This effectiveness can be explained by the property of both frequency and orientation selective which provides a joint optimal resolution in both frequency and spatial domain.

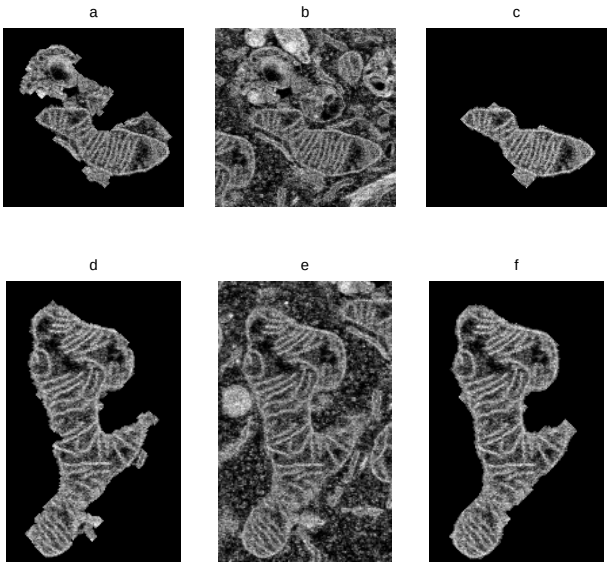

Fig. 5. Fine segmentation examples. *(a)* Detected coarse mitochondrial segmentation object 1. *(b)* Retrieved original cropped region containing object 1. *(c)* Fine segmented of object 1. *(d)* Detected coarse mitochondrial segmentation object 2. *(f)* Retrieved original cropped region containing object 2. *(g)* Fine segmented of object 2.

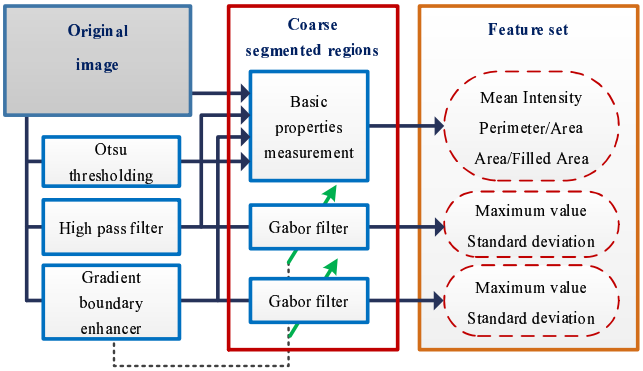

Fig. 6. Feature extraction scheme.

The general 2D Gabor filter function is defined by

$$g_{\lambda,\theta}(x,y) = \exp\left(-\frac{1}{2}\left(\frac{x_\theta^2}{\sigma_x^2}+\frac{y_\theta^2}{\sigma_y^2}\right)\right)\exp\left(j\frac{2\pi}{\lambda}x_\theta\right) \quad (6)$$

where $x_\theta = x\cos\theta + y\sin\theta$ and $y_\theta = -x\sin\theta + y\cos\theta$, λ is the wavelength of the sinusoidal plane, θ is the orientation of the Gabor filter, and σ_x and σ_y are the standard deviations of the Gaussian envelope along the x axis and y axis, respectively. The Gabor filter can be analyzed into even and odd parts by $g_{\lambda,\theta} = g_{\lambda,\theta}^{even} + jg_{\lambda,\theta}^{odd}$. Denote $\gamma = \sigma_y/\sigma_x$ and $\sigma = \sigma_x = \gamma\sigma_y$ then the odd and even parts of the Gabor filter are

$$g_{\lambda,\theta,\gamma}^{odd}(x,y) = \exp\left(-\frac{x_\theta^2+\gamma y_\theta^2}{2\sigma^2}\right)\cos\left(\frac{2\pi}{\lambda}x_\theta\right) \quad (7)$$

and

$$g_{\lambda,\theta,\gamma}^{even}(x,y) = \exp\left(-\frac{x_\theta^2+\gamma y_\theta^2}{2\sigma^2}\right)\sin\left(\frac{2\pi}{\lambda}x_\theta\right) \quad (8)$$

respectively. The half-response spatial frequency bandwidth B is selected by [19]:

$$B = \log_2\frac{\frac{\sigma}{\lambda}\pi + \sqrt{\frac{\ln 2}{2}}}{\frac{\sigma}{\lambda}\pi - \sqrt{\frac{\ln 2}{2}}} \quad (9)$$

The Gabor filter after defined will be convoluted with the input image $I(X,Y)$. The magnitude of Gabor coefficient at a pixel is computed as follows:

$$G_\theta(X,Y) = \left|\sum_{x=-\frac{w}{2}}^{\frac{w}{2}}\sum_{y=-\frac{w}{2}}^{\frac{w}{2}} I(X+x,Y+y)\, g_{\lambda,\theta,\gamma}(x,y)\right| \quad (10)$$

where I is a window of size $w \times w$.

In general, the Gabor coefficient of a pixel can be calculated as a square root combination of coefficients determined by multiple Gabor filters with different orientations. However this computation method will decrease the regional contrast of output coefficients since "out-of-orientation" Gabor coefficients will cause a reduction on the "in-orientation" ones which is usually the biggest Gabor coefficient. Furthermore, high-oriented ridge texture is frequently appeared in mitochondrial regions, while do not exist in other organelles' regions. Therefore, determinating a correct orientation θ for Gabor filter is necessary for enhancing the discrimination between mitochondrial and non-mitochondrial regions.

In this paper, we propose an orientation adaptive Gabor filter for such textural feature extraction. Output Gabor coefficient of a pixel is computed by a Gabor filter of which the orientation θ_{xy} is calculated based on to the pixel's local gradient orientation φ_{xy} in (3) as follows:

$$\theta_{xy} = \varphi_{xy} + \frac{\pi}{2}. \quad (11)$$

In order to reduce the computation of the orientation adaptive Gabor filter, the orientation for Gabor filter at each pixel θ_{xy} is linearly quantized to a certain set of N orientations $\{\theta_k\}_{k=1}^N$ as follows:

$$\theta'_{xy} = \begin{cases} \frac{k\pi}{N} & \frac{(k-1)\pi}{N} < \theta_{xy} \le \frac{k\pi}{N}, k = 1,..N-1 \\ 0 & \theta_{xy} > \frac{(N-1)\pi}{N} \end{cases} \quad (12)$$

Due to the the matching of orientation between Gabor filter and mitochodrial ridge texture, the maximum value of Gabor coefficients of a mitochodrial region will be higher than that of other non-mitochondrial regions. Furthermore, since most of textures of non-mitochondrial regions have more unvarying distribution than that of mitochodrial regions, the standard deviation of Gabor coefficients of mitochondria regions tends to be higher than that of non-mitochondrial ones. For that reason, we consider the maximum and the standard deviation values of Gabor coefficients are the most distinctive features for detecting mitochondria.

In order to implement Gabor features extraction for mitochondiral detection, as shown in Fig. 6, we adopt adaptive Gabor filters to the high pass filtered version and the gradient boundary enhanced version of intracellular images. The reason for this utilization can be explained by the fact that the textural

regions of mitochondria in high pass filtered version and gradient boundary enhanced version are more highlighted than that in the original intracellular image.

2) Basis regional features: Complementing to textural features, we utilize some other basic quantitative parameters for the feature set. For distinguishing mitochondrial region from some darker or brighter regions of other organelles such as vesicles, cytoskeleton, etc, the mean value of the intensity of coarse segmented region is added to the feature set.

In addition, since ridges and boundaries of mitochondria, formed by brighter pixels compared to the remainders, are thinner than those of other organelles, the ratio of mean original intensity of pixels belonging to Otsu thresholded gradient boundary enhanced coarse segmented regions divided by that belonging to Otsu thresholded high pass filter coarse segmented regions is extracted as a feature for distinguishing mitochondrial and non-mitochondrial regions. We denote this term as $MeanHPF/MeanGrad.$ in Fig. 6.

Another feature of the regional ratio of perimeter divided by area, which can help to recognize the filament structures derived from endoplasmic reticulum, golgi apparatus or cytoskeleton organelles, is also utilized. Normally, the ratio of regional perimeter and area of a mitochondrion is higher than that of a filament region. We signify this ratio as $Perimeter/Area$ in Fig. 6.

Besides, it is obvious that the solidity, which is defined by ratio of binary regional area divided by convex area, of a mitochondrial region is differ from the solidity of most of other organelles' regions, except some special touched filament regions. Furthermore, since the filled area of a mitochondrial region is almost equivalent to its convex area while the filled areas of some of special touched filament regions differ from their convex areas, the replacement of convex area by filled area will increase the distinction of the solidity feature between mitochondrial regions and some special touched filament regions. Therefore, the modified solidity which is re-defined by the ratio of binary regional area divided by filled region area, is also utilized for detecting mitochondrial regions. We indicate this modified solidity as $Area/FilledArea$ in Fig 6.

B. Machine learning-based mitochondrial detection

In order to detect mitochondrial regions, we consider multiple types of classifier including *k*-NN, SVM and neural network (NN). The coarse segmented regions is divided into a training set and a testing set. Extracted feature set of the training set is combined with validation data in a learning process. The output system of that learning process, which will be used for detecting mitochondrial regions, is evaluated based on the testing set.

It should be noticed that the proposed feature set for mitochondrial detection is only contained in an 8-dimensional space. Therefore, the resources for training task of the proposed method is much lower than those of many of previous works [11], [12]. However, the proposed feature set still ensure good coverage for detecting mitochondrial regions, since both basis geometrical features and textural features of coarse segmented regions are utilized. Therefore, the proposed method is simple in machine learning implementation aspect.

IV. Experiments

The experiments are conducted with FIB-SEM intracellular images collected from the cancer cell line of a human head and neck squamous cell carcinoma (SCC-61). Fig. 4a shows an example FIB-SEM scan of a cancer cell SCC-61. Compared to the images of CA1 hippocampus and striatum tissues [11] which are also captured by FIB-SEM system, the studied images images are more complicated. Moreover, due to higher resolution, the mitochodrial segmentation task for the studied FIB-SEM images of SCC-61 cancer cell are more difficulty than the mitochodrial segmentation task for IA-SEM images of MNT-1 cells [12], [33], [34] and SBF-SEM images of mouse cerebellum, dentate gyrus, and CA3 hippocampus [35].

In general, the performance of the proposed three-stage mitochondrial segmentation method is mainly decided in the accuracy of the detection stage. Therefore, we focus on analyzing the effectiveness of the proposed detection method in this section.

A. Parameters selection for feature extraction

There is a resonance effect of spacial frequencies of mitochondrial ridge texture and Gabor filter. As a result, the selection of spacial frequency for Gabor filter is very important for making an accurate mitochondrial detector. Herein, we adopt Fourier transform-based frequency analysis method for determining spacial frequency λ of ridge textures of mitochondria. The determination process is illustrated in Fig. 7. A slice cut of a single mitochondrial region, e.g., the solid line as shown in Fig. 7a, is extracted. Fig. 7b plots the spacial intensity series of the slice cut in Fig. 7a. Adopting Fourier transform to the spacial series, we obtain the magnitude spectrum of the spacial series as shown in Fig. 7c. The spacial frequency of the ridge texture is determined to be equal to the first order harmonic component, i.e., the peak at $\lambda = 5$ in Fig. 7c.

It should be noted that the slice cut n Fig. 7a is intentionally selected such that the cut is orthogonal with the ridge texture orientation. In case of a cut slice is "out-of-orientation" with ridge texture, the output frequency may be distorted. Consequently, the output of Gabor filter will strongly depend on the local orientation of mitochondrial ridge texture. This effect also shows the validity and potential of the proposed idea on using Gabor filter with adaptive orientation.

Obviously, the proposed adaptive Gabor filter is designed for resonant with mitochondrial ridge texture. However, a coarse mitochondrial region can also contain some touched parts of other organelles, which can create low values of Gabor coefficient. As a result, the best Gabor feature for mitochondrial detection is the maximum value of Gabor coefficients of coarse segmented region. Next, we investigate the influence of parameters on the mitochondrial detection efficiency of the key detection factor of maximum value of regional Gabor coefficients. Hereafter, we consider high pass filtered version of original intracellular space scans for the investigation. The results are shown in Fig. 8. In order to present the effectiveness of detection parameters, we utilize receiver operating characteristic (ROC) curves, which is the

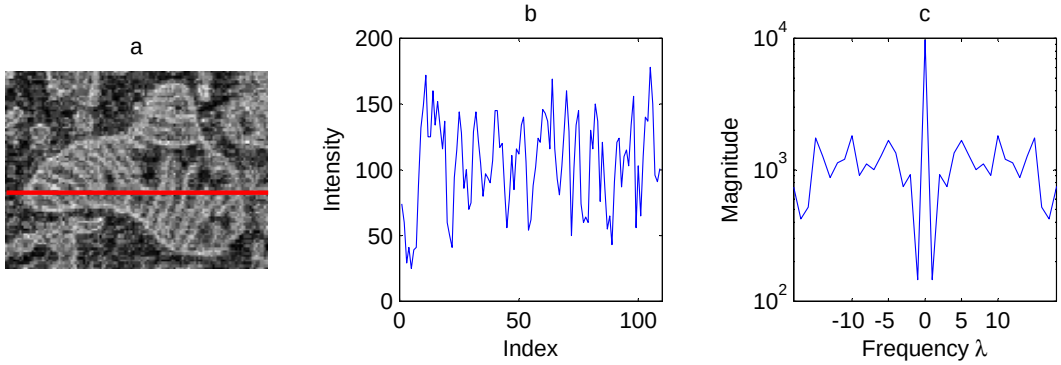

Fig. 7. Spacial frequency determination example. *(a)* A mitochondrial region with a horizontal slice cut. *(b)* Intensity of pixels on the slice cut. *(c)* Fourier transform of intensity series(b).

plot of true positive rate (TPR) and false positive rate (FPR). In this paper, TPR is defined by the ratio of number of correct detected mitochondrial regions divided by the total number of mitochondrial regions in the images. And FPR is defined by the ratio of number of incorrect detected mitochondrial regions divided by the total number of non-mitochondrial regions.

Fig. 8a presents ROC curves of the maximum value of coarse segmented regional Gabor coefficients computed based on the proposed orientation adaptive Gabor filter corresponding to different spacial frequencies when the parameter of window size w and the orientation quantization levels N are fixed at 5 and 24, respectively. As shown in Fig. 8a, the mitochondrial detection ability of maximum regional Gabor coefficient computed by the proposed method depends on the value of spacial frequency. Matching with the previous analysis, the detection performance of maximum regional Gabor coefficient at spacial frequency of $\lambda = 5$, which is equal to the first order harmonic frequency component, is higher than that at other frequencies. This observation proves the effectiveness of choosing correct spacial frequency for mitochondrial detection.

Since for our proposed orientation adaptive Gabor filter, the calculation of local orientation of intracellular images strongly affect to the output Gabor coefficients and hence the detection performance of the maximum Gabor coefficient feature. There are two parameters that influence on the calculation of local orientation of intracellular images. They are the window size w for computing the local gradient orientation and the number of orientation quantization levels.

First, the impact of window size w to the detection performance of the maximum Gabor coefficient feature is presented on Fig. 8b. From the ROC curves corresponding to three value of w of 5, 7, and 9, it can be seen that the value of w do not highly affect on the mitochondral detection performance of the maximum Gabor coefficient feature since the ROC curves are almost the same.

Second, we investigate the effect of number of orientation N on mitochondrial detection performance of the maximum Gabor coefficient features calculated by both the proposed N quantized orientation adaptive and the conventional root mean square N orientations Gabor filter. The results are plotted in Fig. 8c. It can be seen that the accuracy of mitochondrial detection of the maximum Gabor coefficient features of the both Gabor filter will slightly increase along with the increment of orientation number N.

Particularly, it can be also seen in Fig. 8c that the mitochondrial detection accuracy of our proposed orientation adaptive Gabor filter is higher than that of conventional Gabor filter in all case of N. The proposed oriental adaption for Gabor filter following local orientation of mitochondrial ridge texture improves the detection ability for Gabor filter.

Finally, in order to confirm the effectiveness of Gabor filter for mitochondrial detection, we compare the mitochondrial detection ability of our proposed Gabor filter-based textural features including the maximum and standard deviation values of coarse segmented regions with other textural features including homogeneity, contrast, correlation and entropy derived from famous gray level co-occurrence matrix (GLCM). The results is presented in Fig. 8d. Obviously, our proposed features of maximum and standard deviation values of coarse segmented regions outperforms the textural features extracted based on GLCM for mitochondria detection.

B. Machine learning-based mitochondrial detection

Our experiments was conducted on 20 scans of a SCC-61 cell. Half of the images are used for training and the remainders are used for evaluating the trained models. Multiple machine learning methods including k-NN-based, SVM-based and NN-based classifier for mitochondria detection are considered. For k-NN classifiers, we tested with multiple values of k including k = 5, 9 and 15. For SVM-based classifiers, sequential minimal optimization (SMO) [36] and least square (LS) methods are considered for training SVMs. For NN-based classifiers, we performed the training with four configurations of feed-forward back-propagation neural networks, i.e., two configurations with one hidden layer including 10 nodes (net-1) and 20 nodes (net-2) and two configurations with two hidden layers including 10 and 3 nodes (net-3), and 20 and 8 nodes (net-4).

The values of the spacial frequency λ and the number of orientations N of Gabor filters for feature extraction are selected as 5 and 16, respectively, which are reasonable values as analyzed in previous subsection. The value of window size of w, which has shown a low influence to the detection

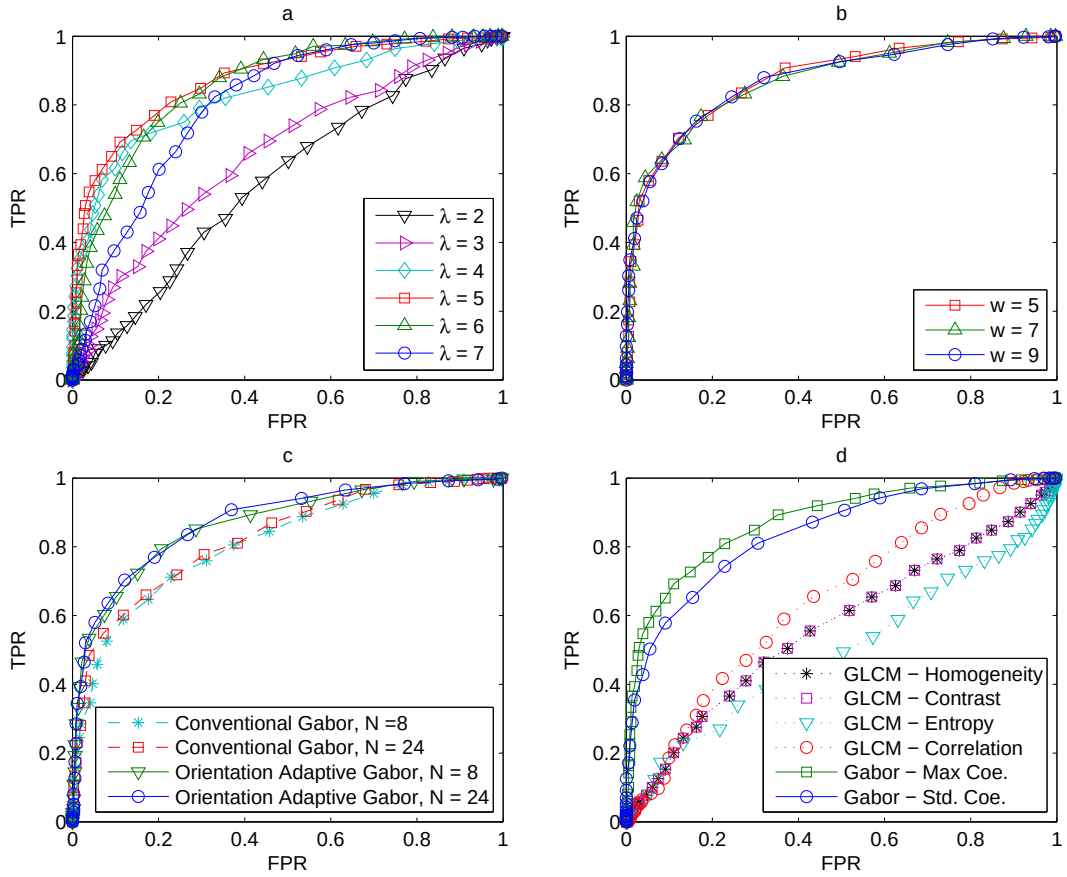

Fig. 8. ROC curves of regional maximum Gabor coefficient in comparison of (a) multiples space frequency λ values, (b) conventional Gabor filter and orientation adaptive Gabor filter, (c) different values of window size w for determining orientation, (d) of other Gabor and gray level co-occurence matrix (GLCM) features.

TABLE I
DETECTION ACCURACY COMPARISON.

	$w=3$, $n=2$	$w=3$, $n=3$	$w=5$, $n=2$	$w=5$, $n=3$	$w=7$, $n=2$	$w=7$, $n=3$	$w=9$, $n=2$	$w=9$, $n=3$
k-NN ($k=5$)	78.94	77.1	76.89	78.94	81.6	81.8	79.55	79.35
k-NN ($k=9$)	80.16	76.89	78.32	79.14	81.19	80.78	81.19	80.16
k-NN ($k=15$)	79.35	79.75	78.94	79.35	82.21	79.96	79.75	79.35
SVM (SMO)	86.3	85.89	87.12	86.50	89.37	**89.98**	**88.75**	88.96
SVM (LS)	**86.91**	**86.71**	**88.75**	**88.14**	**90.18**	89.78	88.55	**89.57**
NN (net-1)	85.89	83.84	87.73	86.30	89.78	87.73	86.09	86.50
NN (net-2)	86.50	85.89	85.28	87.53	87.53	85.28	88.14	87.12
NN (net-3)	84.66	84.25	87.93	86.71	83.03	78.53	85.48	87.12
NN (net-4)	84.66	84.25	87.93	86.71	83.03	78.53	85.48	87.12

performance of the key feature of maximum regional Gabor coefficient extracted from high pass filtered versions of intracellular scans, are set with four different values of 3, 5, 7, and 9 to consider its effect to the final detection accuracy. Similar to w, the values of power order are also selected as 2 and 3 to evaluate its impact to the extracted features of maximum and standard deviation values of regional Gabor coefficients derived from gradient boundary enhanced versions of intracellular scans.

The detection accuracy, which includes true positive and true negative rates, of multiple investigated classifiers are shown in Table I. It can be seen that the influence on final detection performance of window size w value is higher than that of power order n value. This observation can be explained by the fact that the value of w affect to both high pass filtered and gradient boundary enhanced versions of original scans while the value of n only have an effect on the gradient boundary enhanced ones. Similar to spacial frequency λ, there is also a better choice of window size w where the detection performance is higher, i.e., $w = 7$, in this experiment.

For all of investigated cases presented in Fig. I, it can be seen that at least 76% of coarse segmentation regions are classified correctly. Obviously, the method of classifier do influence on the accuracy of detection, i.e., the detection performance generally decreases in the order of SVM-based, NN-based and k-NN classifier. For training selection, it is favorable to choose SVM-based classifier trained by LS method since the detection accuracy of this SVM method is almost the highest

TABLE II
AFFECT OF ORIENTATION NUMBER ON DETECTION ACCURACY.

	ACC	TPR	FPR
$N = 4$	87.32	91.91	20.56
$N = 8$	89.37	92.88	16.67
$N = 16$	90.18	92.88	14.44
$N = 24$	88.55	92.23	17.78
$N = 32$	89.16	92.56	16.67

accurate classifier with approximate 90% of correct detection.

Next, we keep $w = 7$, $n = 2$, and $\lambda = 5$ and change the value of N in order to investigate the affect of orientation number to final detection performance. As shown in Table II, there is a saturation of final detection accuracy (ACC) when N larger than 8. The values of TPR and FPR in such cases are maintained as about 92% and 16%, respectively. These value means that the error rate in identifying mitochondria regions and non-mitochondrial regions are corresponding to about 8% and 16%.

Most of the cases that cause these inaccurate identification belong to the small mitochondrial regions which are falsely merged with large neighbor organelles in coarse segmentation stage, and small non-mitochondrial regions of which the texture can not be detectable. This observation is demonstrated in Fig. 9 where the Fig. 9a indicates coarse segmentation regions of an intracellular image, and Fig. 9a expresses detected coarse mitochondrial regions obtained by an SVM-based mitochondrial detector with $\lambda = 5$, $\gamma = 0.5$, $B = 1$, $w = 7$, $n = 2$ and $N = 16$. In detail, the small mitochondrial regions that are missed due to the affect of large merged neighbor organelles are annotated by (A) and (B). The small non-mitochondrial region that are falsely detected because of the similarity of its texture to mitochondrial small region's texture is marked by (C).

Since most of incorrect detected and miss detected regions are small, the accuracy of our proposed algorithm computed in pixel will be higher than 90%. Therefore, the accuracy of our method can be comparable with the results in [11], [12], i.e., about 95%, while our proposed algorithm is much simpler. Furthermore, it is possible to recovered or discarded correctly the small incorrect detected and miss detected regions by applying 3D reconstruct techniques to adjacent slices where these regions appear clearer to be classified correctly.

V. CONCLUSIONS

We have presented a simple three-stage method for mitochondrial segmentation. The proposed method initially identify mitochondria by coarse segmentation and further identify by a machine learning-based detector. A gradient boundary enhancement is utilize for facilitating the coarse segmentation. A orientation adaptive Gabor filter is adopted for effectively extracting features for mitochondrial detection. The proposed method has illustrated an appropriately simple and high accuracy implementation for the hard problem of segmentation mitochrondria in intracellular space.

ACKNOWLEDGMENTS

We thank Dr. Daisuke Hoshino and Professor Motoharu Seiki of Division of Cancer Cell Research, Institute of Medical Science, University of Tokyo, for providing cancer cell images.

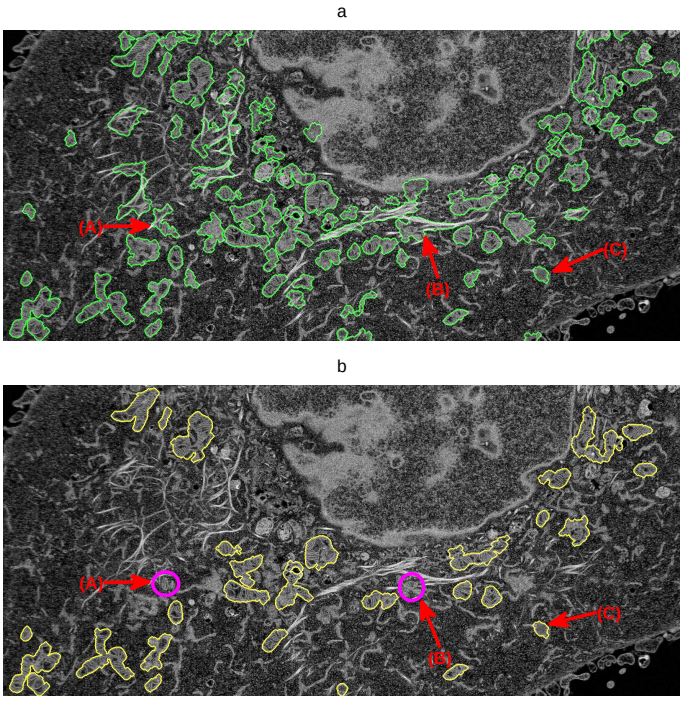

Fig. 9. Mitochondrial detection example. *(a)* Coarse segmentation regions of an intracellular scan. *(b)* Detected coarse mitochondrial regions, obtained by an SVM-based mitochondrial detector with $\lambda = 5$, $\gamma = 0.5$, $B = 1$, $w = 7$, $n = 2$ and $N = 16$, where A and B are annotated for missing mitochondrial regions due to the effect of large neighbor organelles merging with small mitochondrial regions.

REFERENCES

[1] G Kroemer, "Mitochondria in cancer", Oncogene, Vol. 25, pp. 4630-4632,2006.
[2] Gogvadze V, Orrenius S, and Zhivotovsky B.," Mitochondria in cancer cells: what is so special about them?", Trends Cell Biol., 18(4):165-73., 2008.
[3] Douglas C. Wallace, "Mitochondria and cancer", Nature Reviews Cancer, Vol. 12, pp. 685-698, 2012.
[4] Simone Fulda, Lorenzo Galluzzi and Guido Kroemer, "Targeting mitochondria for cancer therapy", Nature Reviews Drug Discovery, Vol. 9, pp. 447-464, 2010.
[5] Wasilewski M. and Scorrano L., "The changing shape of mitochondrial apoptosis", Trends Endocrinol Metab, Vol. 20(6), pp.87-94, 2009.
[6] G. Melino, M. Karbowski, and R. J. Youle, "Dynamics of mitochondrial morphology in healthy cells and during apoptosis", Cell Death and Differentiation, Vol. 10, pp.870-880, 2003.
[7] Campello S. and Scorrano L., "Mitochondrial shape changes: orchestrating cell pathophysiology", EMBO Rep., Vol.11(9), pp.678-84, 2010.
[8] Marina E. Plissiti, Christophoros Nikou, Antonia Charchanti, "Combining shape, texture and intensity features for cell nuclei extraction in Pap smear images," Pattern Recognition Letters, Volume 32, Issue 6, p.p. 838-853, 2011.
[9] Sitansu Kumar Das, Sanjoy Kumar Saha, Dipti Prasad Mukherjee, "Segmentation of multiple objects evolving conditional random field based topology adaptive active membrane," Signal Processing, Vol. 92, p.p. 2341-2355, 2012.
[10] Bjoern Andres, Ullrich Koethe, Thorben Kroeger, Moritz Helmstaedter, Kevin L. Briggman, Winfried Denk, Fred A. Hamprecht, "3D segmentation of SBF-SEM images of neuropil by a graphical model over supervoxel boundaries," Medical Image Analysis, Vol. 16, p.p. 796-805, 2012.
[11] A. Lucchi, K. Smith, R. Achanta, G. Knott, P. Fua, "Supervoxel-Based Segmentation of Mitochondria in EM Image Stacks With Learned Shape Features," Medical Imaging, IEEE Transactions on, vol.31, no.2, pp.474-486, 2012.

[12] Rajesh Narasimha, Hua Ouyang, Alexander Gray, Steven W. McLaughlin, Sriram Subramaniam, “Automatic joint classification and segmentation of whole cell 3D images,” Pattern Recognition, Vol. 42, p.p. 1067-1079, 2009.
[13] Vitaladevuni SN, Sofroniew NJ, Mishchenko Y, Genkin A, Chklovskii DB, Harris K, “Automatic mitochondria detection in electron micrographs,” MIAAB, 2008.
[14] D.J. Stokes, F. Morrissey, B.H. Lich, “A new approach to studying biological and soft materials using focused ion beam scanning electron microscopy (FIB SEM),” Journal of Physics: Conference Series, Vol.26, pp. 50-53, 2006.
[15] E.S. Clark, A.S. Whigham, W.G. Yarbrough, A.M. Weaver, “Cortactin is an essential regulator of matrix metalloproteinase secretion and extracellular matrix degradation in invadopodia,” Cancer Res, Vol. 67, pp. 4227-4235, 2007.
[16] D. Hoshino et al, “Establishment and validation of computational model for MT1-MMP ependent ECM degradation and intervention strategies,” PLoS Comput Biol, Vol.8, 2012.
[17] Canny, J., “A Computational Approach To Edge Detection,” IEEE Trans. Pattern Analysis and Machine Intelligence, Vol. 8(6), pp. 679-698, 1986.
[18] Nobuyuki Otsu, “A threshold selection method from gray-level histograms”. IEEE Trans. Sys., Man., Cyber., Vol. 9 (1), pp. 62-66, 1979.
[19] S. E. Grigorescu, et al., “Comparison of texture features based on Gabor filters,” Image Processing, IEEE Transactions on, vol. 11, pp. 1160-1167, 2002.
[20] J. K. Kamarainen, et al., “Invariance properties of Gabor filter-based features-overview and applications,” Image Processing, IEEE Transactions on, vol. 15, pp. 1088-1099, 2006.
[21] C.-C. Chen and D. C. Chen, “Multi-resolutional gabor filter in texture analysis,” Pattern Recognition Letters, vol. 17, pp. 1069-1076, 1996.
[22] F. Bianconi and A. Fernndez, ”Evaluation of the effects of Gabor filter parameters on texture classification,” Pattern Recognition, vol. 40, pp. 3325-3335, 2007.
[23] X. Wang, et al., “Gabor filters-based feature extraction for character recognition,” Pattern Recognition, vol. 38, pp. 369-379, 2005.
[24] Y. Jonghyon, et al., “Online signature verification using temporal shift estimated by the phase of Gabor filter,” Signal Processing, IEEE Transactions on, vol. 53, pp. 776-783, 2005.
[25] D. Wu, et al., “On the adaptive detection of blood vessels in retinal images,” Biomedical Engineering, IEEE Transactions on, vol. 53, pp. 341-343, 2006.
[26] Y. Zhang and X. Jing, “Spectral analysis based fingerprint image enhancement algorithm,” in Image Analysis and Signal Processing (IASP), 2010 International Conference on, 2010, pp. 656-659.
[27] S. L. Gonzaga de Oliveira and J. Teixeira de Assis, “A methodology for identification of fingerprints based on Gabor filter,” Latin America Transactions, IEEE (Revista IEEE America Latina), vol. 4, pp. 1-6, 2006.
[28] T. Chung-Chih, et al., “Iris Recognition Using Possibilistic Fuzzy Matching on Local Features,” Systems, Man, and Cybernetics, Part B: Cybernetics, IEEE Transactions on, vol. 42, pp. 150-162, 2012.
[29] A. W. K. Kong, et al., “An Analysis of IrisCode,” Image Processing, IEEE Transactions on, vol. 19, pp. 522-532, 2010.
[30] C. Sanchez-Avila and R. Sanchez-Reillo, ”Two different approaches for iris recognition using Gabor filters and multiscale zero-crossing representation,” Pattern Recognition, vol. 38, pp. 231-240, 2005.
[31] S. Dinggang, et al., “Segmentation of prostate boundaries from ultrasound images using statistical shape model,” Medical Imaging, IEEE Transactions on, vol. 22, pp. 539-551, 2003.
[32] S. S. Mohamed and M. M. A. Salama, “Prostate Cancer Spectral Multifeature Analysis Using TRUS Images,” Medical Imaging, IEEE Transactions on, vol. 27, pp. 548-556, 2008.
[33] Heymann, J. A. W., Shi, D., Kim, S., Bliss, D., Milne, J. L. S., and Subramaniam, S. 3D Imaging of mammalian cells with ion-abrasion scanning electron microscopy. Journal of Structural Biology, 166(1): 1-7. 2009.
[34] Murphy, G. E., Narayan, K., Lowekamp, B. C., Hartnell, L. M., Heymann, J. A. W., Fu, J., and Subramaniam, S. Correlative 3D imaging of whole mammalian cells with light and electron microscopy. Journal of Structural Biology, 176(3): 268-278. 2011.
[35] Giuly, R., Martone, M., and Ellisman, M. Method: automatic segmentation of mitochondria utilizing patch classification, contour pair classification, and automatically seeded level sets. BMC Bioinformatics, 13(1): 29. 2012.
[36] J.C. Platt,Sequential Minimal Optimization: A Fast Algorithm for Training Support Vector Machines, in: B.Scholkopf, C. Burges, A. Smola (Eds.), Advances in Kernel Methods - Support Vector Learning, pp. 185-208, 1999
[37] Karel Zuiderveld, “Contrast Limited Adaptive Histograph Equalization.” Graphic Gems IV. San Diego: Academic Press Professional, 1994. 474485.
[38] http://library.thinkquest.org/C004535/mitochondria.html